Behaviour of a masonry arch bridge repaired using fibre-reinforced polymer composites

Behaviour of a Masonry Arch Bridge Repaired Using Fibre-Reinforced Polymer Composites

Y. Tao [a], T. J. Stratford [b], J.F. Chen [c].

[a] PhD student, Institute for Infrastructure and Environment, School of Engineering, The University of Edinburgh, The King's Buildings, Edinburgh, EH9 3JL, UK. Y.Tao @ed.ac.uk

[b] **Corresponding author.**
Lecturer, Institute for Infrastructure and Environment, School of Engineering, The University of Edinburgh, The King's Buildings, Edinburgh, EH9 3JL, UK. Tim.Stratford@ed.ac.uk
Tel: +44 131 6505722. Fax: +44 131 6506781

[c] Reader, Institute for Infrastructure and Environment, School of Engineering, The University of Edinburgh, The King's Buildings, Edinburgh, EH9 3JL, UK. J.F.Chen@ed.ac.uk

ABSTRACT

This paper describes a series of laboratory tests investigating the behaviour of a large model masonry arch bridge repaired with externally bonded fibre-reinforced polymer (FRP) on its intrados. Many similar masonry arch bridges form critical links in the world's transport infrastructure, but they are often not suited to the increased demands of modern traffic loading, especially in ageing arch structures that have suffered structural deterioration. FRP plates, adhesively bonded to the intrados of the masonry arch are a convenient method for strengthening arch bridges. The tests described in this paper demonstrated that FRP strengthening is an effective technique for improving the structural performance of a masonry arch bridge.

A two-span, single-ring semi circular brick arch bridge was tested in this study, complete with fill material. Each of the spans was initially loaded to investigate their response and to establish a four-hinge collapse mechanism, simulating damage prior to strengthening. FRP strengthening was then applied to the two arches, and each of the spans was again tested separately until failure of the strengthening system. The global (load and deflection) and local (crack width and FRP strain) response of the structure was recorded. The FRP strengthening resisted flexural crack opening in the masonry, and hence prevented a four-hinge mechanism collapse. Failure instead occurred when the FRP strengthening debonded from the masonry adjacent to an existing intrados hinge crack. As well as shear debonding adjacent to flexural cracks in the masonry, peel debonding occurred where shear deformation occurred across a masonry crack. Catastrophic collapse did not occur, as the FRP continued to contribute to the load capacity by acting as a tie after the ultimate load had been reached.

KEYWORDS

Masonry arch; FRP; Repair; Experiment; Failure mode; Debonding.

1 INTRODUCTION

Masonry arch bridges are an important part of many countries' rail and road transport infrastructure. Most are historic structures that survive in active service largely due to the inherent stability of the arch form. The combined effects of modern traffic loads (for which they were not designed) and degradation of the masonry mean that some of these bridges suffer from significant damage. It is important to safeguard and extend the life of these structures, especially where arch bridges form critical links in the transport network and where major disruption would result from their closure.

Fibre-reinforced polymer (FRP) systems are increasingly used for bridge repair and strengthening, with particularly widespread application to concrete bridges [1,2]. The FRP is adhesively bonded to the surface of the existing structure, where it provides tensile capacity and restrains the opening of cracks. FRP has the advantages of a low weight to strength ratio, short installation periods and minimal intervention upon the structure [3]. The small thickness of FRP required for strengthening is especially important for historic bridges, as it minimises changes to the bridge's appearance. The application of FRP composites to masonry structures is less well established, although it has been the subject of research and development in recent years [4], demonstrating that FRP can be used to upgrade the structural performance of a variety of masonry elements, and has resulting in design guidance being issued by the National Research Council in Italy [5] and by the American Concrete Institute [6]. Further work is required, however, to apply FRP strengthening to increase the load capacity of masonry arch bridges.

1.1 Masonry arch mechanics

Masonry is an assemblage of bricks or blocks that are joined with mortar. Failure of the masonry is usually governed by the low interfacial strength between the brick and mortar in tension and shear. In a single ring masonry arch bridge, the critical failure mechanism is a four-hinge mechanism (Fig. 1), when the arch is loaded at its quarter span [7,8]. Sliding or crushing mechanisms (discussed further below) are also possible in a masonry arch, but these are unlikely to occur because the critical loads are well above that of the hinge mechanism [8,9]. In multi-ring arch bridges, ring separation may become critical.

Fig. 1 shows only the arch, as this is the principal load-carrying member of the bridge. However, the arch does not act in isolation: fill is placed above the arch to provide the required top profile, and this is retained by spandrel walls on either side of the bridge, which extend upwards to act as parapets. The bridge abutments both retain the fill material and prevent springing of the arch.

The critical hinge mechanism involves flexural cracks that open along the mortar joints at the hinge locations. These cracks alternate between the intrados and extrados of the arch, as shown in Fig. 1 [8]. Externally bonded FRP can be used to provide tensile capacity and restrain the opening of the cracks, just as for concrete strengthening. Ideally, the FRP would be bonded to both the intrados and extrados of the arch so that both types of crack can be effectively restrained; however, the extrados is usually not

accessible without removing the fill material. As a consequence, only intrados FRP strengthening can usually be applied to a masonry arch bridge.

1.2 FRP strengthening for masonry structures

Much of the research into FRP strengthening for masonry has so far studied walls subjected to in-plane [10,11,12,13,14] and out-of-plane [13,15,16,17,18,19] loading. The out-of-plane bending of walls is relevant to the four-hinge mechanism failure in arches, as there is a similar interaction between the FRP, the opening of flexural cracks in the walls, and the reliance upon the adhesive joint between the FRP and the masonry. Wall elements, however, do not include the curvature present in arches.

There has also been prior research upon FRP applied to arches and vaults. Barrel vaults are similar in form to arches; however, unlike arches, the extrados is often accessible for strengthening, whereas it might not be acceptable to apply FRP to the visible intrados of the vault. FRP composites restrain the opening of flexural cracks in an arch, but they do not prevent crack formation [9,20]. By restraining the growth of flexural cracks it is possible to prevent the hinge mechanism mode of failure [4,9], and it has also been demonstrated that the lateral abutment thrust is reduced [21,22]. Increasing the hinge mechanism failure load, however, means that other failure mechanisms may become more critical. Five characteristic failure modes have been identified for FRP-strengthened arches in previous work [4,9,23,24]:

- the hinge mechanism (local rotation about flexural cracks);
- sliding along the mortar joints (shear cracks);
- compressive failure of the masonry;
- tensile rupture of the FRP; and
- separation of the FRP from the masonry (debonding failure of the adhesive joint).

Debonding of the strengthening occurs in the weakest link between the FRP, adhesive, and masonry; this is often slightly below the surface of the masonry [9,12]. As well as complete detachment of the strengthening from the masonry (the last failure mode), debonding plays an important role in the first two failure modes. The FRP strengthening bridges local flexural or shear cracks, but as the cracks grow a portion of the adhesive joint fails adjacent to the crack, the extent of which increases with crack opening. It is the interaction of local debonding, crack opening, and compatibility of the partially debonded FRP with the curved surface of the masonry that determines how well the FRP restrains the hinge rotation at the position. An understanding of the debonding mechanism is therefore an important part of understanding the failure of FRP strengthened masonry arches.

Adding FRP strengthening to a masonry arch thus changes its failure mode. An arch without strengthening forms a kinematic mechanism. The addition of FRP, however, allows tension to be carried across an opening crack, and the strength of the component parts must be examined, in a similar manner to the sectional analysis of a curved reinforced concrete beam. Several researchers have

developed analytical predictions of the ultimate strength of FRP strengthened masonry arches. Some can simplistically be described as discrete block models, in which the contact properties between the FRP and masonry and between adjacent masonry blocks are modelled [20,26]. Other analyses take a sectional analysis of the strengthened arch as their starting point [9,23,24,25]. This broad classification, however, is rather crude: all of the previously proposed analysis methods combine aspects of mechanism failure and component failure to different extents, reflecting the possible failure modes in an FRP strengthened arch. The focus of the current paper is upon experimental work; hence, these analytical models are not explored in further detail.

Prior research has thus demonstrated that the load carrying capacity of a masonry arch can be increased using externally bonded FRP strengthening; however, a clear understanding of the failure mechanics (and in particular the bond between the FRP and the masonry) has yet to be fully developed. The tests described in this paper examine both the global response of a FRP strengthened masonry arch bridge and the local mechanics of failure.

2 EXPERIMENTAL METHODOLOGY

Tests were conducted upon a model two-span masonry arch bridge. In outline, the tests involved:

- Loading each of the masonry arches in turn (north first) at quarter-span until a four-hinge mechanism formed so as to simulate damage to the arch prior to strengthening.
- Application of the FRP strengthening.
- Testing each of the arches in turn until failure of the strengthening system occurred, but without complete collapse of the structure.
- A final destructive test upon the south arch, resulting in complete collapse.

The methodology is described in more detail in the following sections.

2.1 General arrangement

A two-span masonry arch bridge model was built in the Structures Laboratory of the University of Edinburgh in 1996. The two semi-circular single-ring arches (2080mm span, 1040mm rise and 1680mm width) were constructed from concrete bricks (100×65×215mm) and cement mortar (nominally 15mm thick), as shown in Fig. 2. The bricks were laid in a stretcher bond with the bed joints across the arch width.

The arches were covered by a dry sand fill to a height of 350mm above their crowns. The fill was contained by plastic sheeting and timber spandrel walls and abutments; the timber walls were not in contact with the arches so did not directly affect their structural performance. The abutments were supported using laboratory steelwork attached to the laboratory strongfloor, and were effectively rigid. It should be noted that no previous tests have been carried out on FRP strengthened arches that included fill material.

The arches were originally used to investigate their deformation under various positions of concentrated load and cracks had already initiated in the arch, at the same position as the four-hinge mechanism investigated in the current tests. The current tests were conducted on the arches in 2008.

2.2 Arrangement and application of the FRP strengthening

Pre-cured CFRP strengthening plates were bonded to the surface of the arches. Preformed plates were chosen because of their suitability for on-site installation and because their existing stiffness gives them a smooth profile. Wet lay-up or pre-impregnated strengthening could also be used (and may result in thinner sections that reduce the possibility of debonding); the choice is likely to be governed by the practicality of working with these materials in the environment of a construction site.

A commercial FRP system intended for structural strengthening was used that comprises 100mm wide unidirectional pultruded carbon fibre-reinforced polymer (CFRP) plates and a two-part ambient-cure epoxy adhesive. An initial assessment of the quantity of strengthening to apply to the arches was made using the method described by Chen [25]. Three FRP plates were distributed across the intrados of the north arch, and six plates were similarly applied to the south arch. The FRP plates were labelled P_{N1} to P_{N3} and P_{S1} to P_{S6}, from east to west, and were positioned as shown in Figs 3 & 4.

Prior to strengthening, sharp irregularities in the surface profile of the arch were removed by grinding, and the bonding surface was cleaned through a combination of grinding, wire brush, dry vacuum and solvent cleaning. An epoxy primer was applied to seal the porous masonry, and the plates were then bonded to the arch according to the manufacturer's instructions. The adhesive was nominally 2mm thick, but this thickness varied considerably due to the profile of the arch. Temporary support was provided to the plates for 24 hours during the initial cure of the adhesive.

2.3 Material properties

The properties of the masonry materials were determined from specimens cut from the arches after the final test. Tests were conducted to determine:

- the compressive strength (f_{cb}), elastic modulus (E_b) and flexural tensile strength (f_{tb}) of the masonry bricks;
- the compressive strength (f_{cm}), elastic modulus (E_m) and flexural tensile strength (f_{tm}) of masonry assemblages; and
- the initial shear strength (f_{v0}) and the internal angle of friction (α) of a bed joint, derived from 'triplet' tests, as shown in Fig. 5.

Table 1 lists the masonry material properties obtained from these tests. This table also lists the direction of the property being tested relative to the direction of the bed joints. 'Parallel to the bed joints' being across the width of the arch, and 'perpendicular to the bed joints' being in the circumferential direction.

The test methods were based upon the British Standards listed in Table 1 in so far as was possible given the specimens that could be cut from the arches.

The sand fill had a density of 1520kg/m^3 and an internal friction angle of 33°.

Based upon the manufacturer's datasheet values, the FRP plates had a nominal cross-section of 100×1.4mm, Young's modulus of 170GPa and tensile strength of 3100MPa. The epoxy adhesive had a Young's modulus of 10GPa and minimum shear strength of 17MPa.

2.4 Loading and instrumentation

A line load was applied across the width of the arches. The load was applied to the top of the fill, at the critical quarter-span position above each arch in turn (Figs 2 & 3). The load was applied by means of three 10-tonne hydraulic jacks, attached to a portal reaction frame that was bolted to the laboratory strong floor. A steel beam beneath the three jacks spread the applied load into a line, and a timber plate distributed this load over a wider area. A 300mm wide timber plate was used prior to strengthening the arches; after strengthening the width of the timber was increased to 600mm (as indicated in Fig. 2) to prevent the load punching into the fill material.

The load was applied using a hand pump and was controlled manually by observing the output from three load cells positioned beneath the jacks. Displacement transducers were used to measure radial displacements (δ) of the arch along a line halfway across their width (Figs 3 & 4); radial displacement was measured rather than vertical displacement because it dominates the four-hinge arch mechanism (Fig. 1). A sequence of digital photographs was taken on either side of the arch to allow crack formation to be monitored.

When the strengthening was applied, the load cells and displacement gauges were augmented by electrical resistance strain gauges and crack width gauges. 25 strain gauges were bonded to the FRP at the locations shown in Fig. 4 (12 under the north arch and 13 under the south arch) to measure the longitudinal strain (ε) on the centreline of the plates. The majority were installed on the central FRP plate, so as to record the variation in axial strain along the plate, with four gauges on the outer plates at the position of the hinge cracks created during the initial stage of loading. Five crack width gauges were used to measure crack openings (w); four were positioned over the hinge cracks on the arch being tested, and the fifth gauge was placed over a hinge crack in the adjacent arch (Fig. 4). The gauges were placed 25mm from the open end of the crack.

Not all of the instrumentation was used in every test. Tests on the north arch used:

- 5 displacement transducers (δ_{N1} to δ_{N5}) under the north arch and 2 under the south arch (δ_{S1} and δ_{S2});
- all of the strain gauges (ε) under the north arch, but none of those under the south arch; and

- 4 crack width gauges (w_{N1} to w_{N4}) on the north arch, with 1 (w_{S1}) on the south arch.

The instrumentation was reversed for the tests on the south arch.

3 TEST RESULTS

This section presents the results for the tests carried out prior to strengthening, the tests carried out after strengthening, and the final collapse test on the south arch.

3.1 Tests prior to strengthening

Prior to strengthening, the north arch and south arch were individually loaded until a four-hinge mechanism had been established. Figure 3 shows the locations of the hinge cracks. The cracks are labelled in the form C_{NA}, where the first subscript identifies the arch (North or South). The second subscript identifies the crack, using numbers for intrados cracks (e.g: C_{N1}) and letters for extrados cracks (e.g: C_{NA}). Typical intrados and extrados cracks are shown in Fig. 6.

Fig. 7 plots the load-deflection responses of the north and south arches. The response of the arches prior to strengthening is shown in the lower part of the responses. The load-deflection response is approximately bi-linear, with a change in stiffness when the hinge mechanism was established. This occurred at similar loads in the two arches: 35kN for the north arch, and 39kN for the south arch. Upon further loading, the arch behaved as an anti-symmetric four-hinge mechanism. The displacements were consistent with hinge mechanism.: the radial displacement was close to zero at the crown of the arch (δ_{N3} & δ_{S3}), outwards (positive) in the region of the extrados cracks (δ_{N4}, δ_{S4}, δ_{N5} & δ_{S5}), and inwards (negative) in the region of the intrados cracks (δ_{N1}, δ_{S1}, δ_{N2} & δ_{S2}). Minimal deflections were recorded in the adjacent unloaded arch, indicating little interaction between the two arches.

A number of unload-reload cycles were conducted, only the last of these is shown in Fig. 7. The north arch was loaded to 46.2kN and the south arch to 49.7kN, when it was deemed that the arches were approaching their unstrengthened load capacities. Irrecoverable damage occurred as the hinge cracks opened, resulting in residual deformations once the load had been removed. The cracks were allowed to open wider on the north arch, resulting in greater residual displacements than for the south arch.

3.2 Tests After strengthening

3.2.1 Overview of the test results

After strengthening, each of the arches was loaded in turn until the ultimate limit state was reached due to debonding failure of the strengthening system. In section 1.2, five failure mechanisms were identified for an FRP-strengthened masonry arch. A combination of three of those failure mechanisms occurred during the current tests: the hinge mechanism (involving rotation about flexural cracks), the sliding mechanism (involving shear along mortar joints), and debonding of FRP. In both arches, the tests were terminated after sudden debonding of the FRP from the masonry in the vicinity of the local

masonry cracks. This debonding resulted in a sudden drop in the load-carrying contribution of the strengthening, and determined the maximum load capacity of the strengthened arches; however, the FRP did not completely separate from the masonry, and retrained some post-peak load capacity.

In this section, the performance of the arches is reported and discussed in terms of its load-deflection behaviour, failure mechanism, crack width evolution, and FRP strain response. Each of the tests on the arches is discussed in turn.

3.2.2 North arch test after strengthening

The north arch was strengthened using 3 FRP plates (Fig. 4a). The following data were recorded during the test on the north arch:

- Load vs. radial deflection response (Fig. 7a). Note that the displacement transducers were reset at the start of this test, so the figure plots additional displacement and does not include the residual displacements from the end of the test prior to strengthening.
- Crack width development (Fig. 8a). The figure plots the crack displacement at the mouth of the crack, calculated from the displacement at the gauge position by assuming that the crack rotates about the opposite fibre of the arch.
- The development of strain in the FRP plates, presented as a load-strain response for the gauges coincident with cracks C_{N1} and C_{NA} in Fig. 9a, and as profiles of strain in the central FRP plate (P_{N2}) for different applied loads in Fig. 10a.
- The failure mode of the arch, showing the location of cracks in the masonry and the extent of debonding of the FRP strengthening form the masonry. This is presented as a plan view along the developed length of the arch in Fig. 11a, and as sections taken along the strengthening plates in Fig. 12.

Initial loading (0 to 50kN)

The load-displacement response of the strengthened arch was stiffer than for the arch prior to strengthening. The FRP bridged the cracks, and resisted their opening.

As discussed in section 1.2, a four-hinge mechanism (with an extrados crack at C_{NA} and an intrados crack at C_{N1}) was established in the arch prior to strengthening (Fig. 3). After strengthening, the same four-hinge mechanism opened up during the initial stages of loading, as shown by the positive crack widths in Fig. 8a. The strains in the FRP plate at the crack positions are also consistent with the hinge mechanism, giving tension at the intrados crack and compression at the extrados crack (Fig. 9a) during the early stages of loading.

The north arch test had negligible affect upon the unloaded south arch at any point during the test: no deflection was recorded by gauges δ_{S1} or δ_{S2} in the south arch, and crack w_{S1W} did not widen.

The four-hinge mechanism can also be seen in the strain profile along FRP plate P_{N2} (Fig. 10a). For loads less than 110kN, the peak strain is recorded in gauge $\varepsilon_{N2\text{-}5}$, coincident with the intrados crack C_{N1}. The strain decreases to either side of this crack, with a compressive strain at $\varepsilon_{N2\text{-}8}$, coincident with the extrados crack C_{NA}. The load-strain response shows that there was little variation in the load carried by each of the plates, with only a small difference in the plate strains up to 110kN.

Increased loading (50 to 110kN)

A true four-hinge mechanism only acted up to a load of around 50kN (approximately the capacity of the original arch without strengthening). Above this load, intrados crack C_{N1} continued to open as the load was increased (Fig. 8a), as did the strain in the FRP at this location (Fig. 9a). The extrados cracking, however, became more distributed. Extrados crack C_{NA} started to close up (the crack widths in Fig. 8a and FRP plate strains in Fig. 9a returned to zero), at the same time as extrados cracks C_{NB} and C_{NC} (Figs 11a & 12) formed and opened up. A consequence of the more distributed cracking was that the arch no longer deflected in an anti-symmetric mode (Fig. 7a): the crown (δ_{N3}) displaced inwards, and the outwards deflections of the arch were greater than the inwards deflections.

At loads above 80kN, there are frequent fluctuations in the load-deflection, load-strain and load-crack width graphs (Figs 7a, 8a, 9a). These fluctuations were accompanied by audible damage events. The exact nature of the damage could not be observed. This might have been caused by a combination of micro-cracking and softening of the FRP to masonry interface (either within the adhesive, the masonry surface, or (unlikely) within the FRP plate), and damage elsewhere in the masonry, such as cracking in the mortar joints and local crushing of the masonry in compression in the hinge region. The progressive build up of damage within the arch led to softening of the load-deformation response. Other possible causes may include the slip-stick behaviour between the sand fill and the arch, or localised intermitted local failure planes formed in the sand fill, both leading to redistribution of pressures on the arch and thus fluctuations on the response curves.

All of the crack width gauges except w_{N1W} were removed at a load of 100kN to avoid damage to the gauges.

Debonding of the FRP from the masonry (above 110kN)

Additional damage continued to occur within the arch as the applied load was increased beyond 110kN. The micro-cracks that had formed up to this point coalesced to form macro-cracks, particularly along the masonry to FRP interface, which resulted in sudden debonding of portions of the FRP from the masonry.

A number of significant debonding events can be picked up from the plots of strain and deflection:

- At 116kN, the central FRP plate (P_{S2}) partially debonded along a short distance either side of intrados crack C_{N1}. This can be seen in the load-strain response (Fig. 9a), in which there is a

small sudden drop in strain at the central plate ($\varepsilon_{N3\text{-}1}$), and in the strain profile (at 119kN in Fig. 10a), in which there is a sudden increase in strain at the gauges adjacent to the crack ($\varepsilon_{N2\text{-}4}$ and $\varepsilon_{N2\text{-}6}$), indicating debonding along this length.

- At 123kN, a second debonding event resulted in a dip in the load-deflection curves (Fig. 7a). This was due to further debonding of the central plate, as shown by the second sudden but far bigger drop in strain in plate P_{N2} (Fig. 9a).
- The partial debonding of the central plate from the masonry required the outer plates to pick up additional load and undergo higher strains (Fig. 9a). Consequently, the third significant debonding event occurred in the plate that carried the highest strain (P_{N3}) at a load of 129kN, as can be seen on the load-strain plot for plate P_{N3} (Fig. 9a).
- At 132kN, all three plates debonded simultaneously along a substantial length. This resulted in a sudden increase in deflection and crack widening, a drop in the FRP strain and consequently a drop in the load carried by the arch (Figs 7a, 8a and 9a).

At plates P_{N2} and P_{N3}, debonding occurred on both sides of the flexural intrados crack C_{N1} (Figs 11a & 12). On the east side of the arch (plate P_{N1}), however, a shear crack formed through the masonry at the crown of the arch, which joined the intrados crack C_{N1} between plates P_{N1} and P_{N2} (Figs 11a & 12). This shear crack caused plate P_{N1} to debond from the masonry on only one side of the crack, in a peeling mode that was compatible with the shear deformation across the crack (Fig. 13a).

Residual load and deformation

Failure of the FRP strengthening was caused by simultaneous debonding of the three FRP plates described above. However, it should be noted that the FRP had not completely separated from the masonry and still bridged across the cracks and helped prevent collapse of the arch. The residual load carried by the north arch after debonding was 64.8kN, a value that was dependent upon the stiffness of the hydraulic loading system. Fig. 7a also shows that there were substantial residual radial deformations after unloading.

3.2.3 South arch test after strengthening

The strengthened south arch behaved in a broadly similar manner to the north arch; however, more FRP was applied to the south arch (6 FRP plates, Fig. 4b). Similar data were recorded as for the north arch:

- Load vs. deflection response (Fig. 7b).
- Crack width development (Fig. 8b).
- FRP plate strains, in terms of load-strain at gauges coincident with cracks (Fig. 9b) and strain profiles along the central plate (Fig. 10b).
- The failure mode of the arch, in plan view along the arch developed length (Fig. 11b), and sections along the plates showing the initial debonding event (Fig. 14) and the final failure (Fig. 15).

Initial loading (0 to 50kN)

During the early stages of loading, the arch behaved as a true four-hinge mechanism, with crack opening at both the intrados (C_{S1}) and extrados (C_{SA}) cracks that were established prior to strengthening (Fig. 8b). As for the north arch, the FRP plate strains were tensile adjacent to intrados crack and compressive adjacent to the extrados crack (Figs 9b & 10b), and the load-deflection response was stiffer than the unstrengthened arch (Fig. 7b).

Increased loading (50 to 250kN)

As the load was increased above 50kN (the approximate unstrengthened arch capacity), extrados crack C_{SA} started to close up (Fig. 8b), and the formation of a second extrados crack C_{SC} was observed (Fig. 11b). This modified four-hinge mechanism is consistent with the distributed extrados cracking seen in the north arch. The FRP remained in compression at extrados crack C_{SA} throughout the test (Fig. 9b).

The equal crack widths to either side of the arch (Fig. 8b) and similar FRP strains at the different plates (Fig. 9b) indicate uniform load carrying across the width of the arch. Fig. 8b also shows that the width of the intrados crack C_{N1} on the north arch reduced as the south arch was loaded, indicating some interaction between the two arches. The north arch was severely damaged after FRP debonding failure and contained wide cracks during the south arch test, so it is not surprising that it was much more sensitive to load than the south arch.

The strain profile along the central plate P_{S4} had its peak at the intrados crack C_{S1} (gauge $S_{S4\text{-}6}$) for loads up to 200kN. As expected, the strain drops away to either side, with compressive strains at the extrados crack locations.

At 210kN, a new intrados crack C_{S2} formed in the arch two bricks away from the original crack C_{S1} on the east side of the arch (Figs 11b & 16). The crack could be seen to cross the first two strengthening plates (P_{S1} & P_{S2}), and was not present under the two western-most plates (P_{S5} & P_{S6}), but it was not clear whether the crack extended across the two central plates (P_{S3} & P_{S4}) because it was not safe to inspect the underneath of the arch at these high load levels. The formation of this intrados crack increased the rate of strain increase in plate P_{S1} (which bridged the new crack) with loading ($\varepsilon_{s1\text{-}1}$ in Fig. 9b) and increased the rate of crack closure (Fig. 8b). The former phenomenon is consistent with the findings of recent research that shows that the bond resistance is increased when an FRP plate bridges multiple cracks in a concrete beam [33,34]. The location of the peak strain in plate P_{S4} shifted towards the new crack at the same time, suggesting that the new crack may have extended under this plate.

There are frequent fluctuations in the load-deflection and load-strain graphs (Figs 7b & 9b) above 200kN. Just as for the north arch, these indicate progressive damage to the masonry and masonry-FRP interface, initially as micro cracks that cause material softening.

Debonding of the FRP from the masonry (above 250kN)

Damage accumulation along the masonry-FRP interface resulted in sudden debonding of the FRP from the masonry:

- The first significant debonding event occurred at a load of 250kN, when plate P_{S2} debonded over a short length to either side of the two intrados cracks (C_{S1} and C_{S2}). The extent of debonding at this stage is shown in Fig. 14; the other five FRP plates remained bonded to the masonry. Debonding was accompanied by a drop in the load-displacement response (Fig. 7b), an increase in crack opening on the east side of the arch (Fig. 8b), and an increase in the strain in plate P_{S1} (Fig. 9b), which picked up some of the load shed by plate P_{S2}.
- The capacity of the strengthened arch was reached at 254kN, when debonding occurred along a substantial length of all of the FRP plates. It was not possibly to determine whether failure initiated in one plate in particular; all six plates appeared to debond simultaneously. However, the strain profile (Fig. 10b) shows that the peak FRP strain at the intrados crack did not increase as the load was increased from 250 to 254kN, and that the debonded region expanded to either side. Failure of the FRP strengthening caused a sudden increase in deflection and a drop in the load carried by the arch (Fig. 7b).

The details of the masonry cracking and FRP debonding varied across the width of the arch, as shown in Figs 11b & 15. (It was not possible to determine the full extent of the extrados cracks C_{SC} and C_{SD} as they were beneath the sand fill). Flexural cracking of the masonry led to failure at plates P_{S1}, P_{S2}, P_{S3} & P_{S4} (the east and centre of the arch), where the FRP debonded on both sides of the critical crack. The debonded length was approximately the same at all of these positions. Plate P_{S4} (typical of debonding across a flexural crack) is shown in Fig. 13b.

On the west side of the arch, failure was due to a combined flexure-shear failure deformation along crack C_{S1}, as shown in Fig. 17. Consequently, P_{S5} debonded from the masonry on one side of the crack by peeling; P_{S6}, however, debonded to either side of this mixed-mode crack.

Residual load and deformation

The residual load on the south arch after the FRP strengthening had failed was 91kN, and residual radial displacements of up to 18mm remained after unloading (Fig. 7b).

3.3 Collapse test on the south arch

The arches were completely unloaded after the debonding failure of the FRP strengthening so that the instrumentation could be removed. The south arch was reloaded to determine its collapse mode and strength. Digital image correlation (using geoPIV software [35]) was used to determine the radial deflections at the same positions as the displacement gauges (except for δ_{S1}, which was not visible behind the loading frame), allowing the load-deflection response of the arch to be plotted in Fig. 18.

The FRP plates debonded from the arch over a considerable length when the strengthening failed (Fig. 11), but they still remained attached. During the collapse test they acted as ties that bridged the cracks in the masonry and contributed to the load carrying capacity of the arch. The debonded length of the FRP ties increased as the arch was re-loaded, accompanied by the opening of hinge cracks with the masonry. The FRP tie action allowed the arch to carry 113kN, substantially higher than the strength of the arch prior to strengthening (49.7kN). Large deformations were observed at this load (Fig. 18), during which the FRP ties gradually debonded from the masonry arch.

Final collapse occurred when the FRP strengthening completely separated from the masonry and the arch collapsed in a hinge mechanism.

4 DISCUSSION

4.1 The effectiveness of the FRP strengthening system

4.1.1 Load capacity

The FRP strengthening plates significantly increased the load capacities of the north and south arches. The capacity of the north arch (strengthened with 3 plates) was increased by 285%, from 46.2kN to 132kN. The capacity of the south arch (strengthened with 6 plates) was increased by 510%, from 49.7kN to 254kN. The four-hinge collapse mechanism can therefore be prevented and the load capacity of the arch increased substantially using externally-bonded FRP strengthening.

It should be noted, however, that such a large increase in capacity is unlikely to be allowed in design; the Concrete Society [2], for example, require the structure to carry the unfactored loads without strengthening, to avoid catastrophic collapse due to unforeseen damage to the strengthening. Furthermore, the current work was carried out upon a single-ring arch, and not a multi-ring arch as found in many real structures. Ring separation failures may occur in strengthened multi-ring arches, especially as the FRP can only be applied to the intrados ring of the arch. Other appropriate strengthening would be necessary if ring separation becomes critical.

4.1.2 Strengthening mechanisms and modes of failure

The strengthening acted in the same manner in both arches: the FRP bridged the hinge cracks and resisted flexural opening. By resisting the four-hinge mechanism, the FRP allowed additional cracks to form within the arch because it allowed the line of thrust to move outside of the arch ring; in both arches, an additional extrados crack (C_{NC}, C_{SC}) and additional intrados crack (C_{N2}, C_{S2}) formed adjacent to the original cracks (Figs 12 & 15). It is worth noting that additional extrados cracks formed despite the fact that the FRP was applied only to the intrados of the arch. However, it remains unclear whether (and if any, how much) the FRP strengthening contributes to the shear capacity of the arch ring. In both arches shear deformation occurred across masonry cracks at failure (Figs 12 & 15).

The two arches differed only in the number of strengthening plates applied to them, and the fact that the north arch was tested prior to the south arch. Using twice as many FRP plates on the south arch resulted in smaller crack widths compared to the north arch (Fig. 8).

Failure of the FRP strengthening system occurred when the FRP plate debonded from the masonry at an intrados plate beneath the loading position. For both arches, this occurred when the strain in one of the FRP plates reached about 2250 μstrain (Fig. 9). This is in good agreement with the debonding strain predicted by Chen and Teng's [36] anchorage model, using the material properties of the masonry assemblage in place of concrete. This predicts that debonding occurs at a strain of 2430 μstrain for the north arch (with 3 strengthening plates), or 2164 μstrain for the south arch (with 6 strengthening plates). This result also agrees with the anchorage model by De Lorenzis and Zavarise [37], who demonstrated that the curvature does not significantly affect the load at the onset of peeling.

There was considerably less warning of failure of the strengthening system for the south than the north arch, with far less separation between first debonding of the FRP and the capacity of the strengthened arch (Fig. 7). As previously noted, there was a series of debonding events in the north arch above 116kN, in plate P_{N2} and P_{N3}, allowing the load to be re-distributed between the strengthening plates before failure of all three plates simultaneously at 132kN (Figs 9a & 10a). In the south arch, however, there was only one debonding event prior to failure and very little re-distribution of load (Figs 9b & 10b), a consequence of the higher reinforcement ratio using a brittle material.

There were also differences in the crack opening behaviour in each arch. In both arches, the original extrados crack (C_{NA}, C_{SA}) initially opened (Fig. 8) and the FRP at this location was consequently in compression (Fig. 9). As the load increased, however, the width of this crack gradually reduced (Fig. 8), partly due to the formation of neighbouring extrados cracks (e.g.: C_{NC}, C_{SC}). (Note that negative crack widths in Fig. 8 indicate a reduction of the crack width relative to its original width; the crack surfaces were not in contact; i.e. the crack was not fully closed). In the south arch, the FRP at the extrados crack remained under compression, but in the north arch it changed to tension (Fig. 9). It is difficult, however, to attribute this difference in behaviour to the different number of strengthening plates applied to the arches; it is possible that some of the sand fill material had entered the crack in the north arch, and that this acted as a pivot that put the FRP into tension as the crack tried to close.

Following the initial failure of the strengthening system, the FRP did not completely separate from the arch, but acted as ties that continued to contribute to the load carrying capacity of the arch. The ties gradually debonded from the masonry as the hinge cracks grew, giving a degree of ductility albeit at a load lower than the peak capacity of the strengthened arch. This gradual debonding is consistent with the behaviour predicted by an analysis developed by De Lorenzis and Zavarise [38].

4.2 Debonding along the FRP to masonry interface

Brittle debonding of the FRP from the masonry is critical in the failure of FRP strengthened masonry arches. Debonding occurs in the weakest link of the FRP to masonry interface. Close to the hinge crack,

failure occurred within the masonry, leaving a layer of brick (approximately 2mm thick) and mortar (approximately 10mm thick) attached to the plates. Further away from the hinge, failure occurred within the surface of the FRP plate, leaving some of the plate fibres attached to the arch (Fig. 13b). In neither case did failure occur within the bonding adhesive, demonstrating that the surface preparation and FRP installation work were correctly carried out.

The two different locations of debonding are indicative of two different modes of debonding. Debonding occurred within the surface of the FRP in regions where peel debonding was significant, due to the low transverse strength of the FRP plate. Where shear debonding dominated, however, failure occurred within the surface of the masonry.

- Shear debonding dominates close to a flexural hinge crack (such as C_{S2} crossing plate P_{S2}, Fig. 15b). Load is transferred between the FRP and the masonry predominantly by shear stress across the adhesive interface.
- Peel debonding dominates to one side of a shear or mixed mode flexure-shear crack (such as C_{N2} crossing plate P_{N1}, Fig. 12a). Shear across the crack requires normal (peel) stresses to be carried across the adhesive.
- Peel also plays an important part once the FRP has debonded over a substantial length and the FRP forms a tie, due to the angle at which the plate joins the intrados of the arch.

This paper has focused upon the experimental results from the arch tests, but additional work is being carried out to interpret and model the debonding failure in detail.

4.3 Alternative strengthening materials

Whilst the arch bridges were strengthened with externally bonded FRP plates on their intrados, they may be strengthened in a similar manner using other suitable materials, such as near surface mounted (NSM) bars made of FRP or stainless steel bars. The behaviour of these systems is likely to be similar to externally bonded FRP, although the bond characteristics will differ. It must also be noted that, whilst the FRP strengthening is very effective for enhancing the loading capacity due to the four hinge mechanism failure, other failure modes such as shear and ring separation may become critical in a strengthened bridge they must also be carefully considered in design.

5 CONCLUSIONS

The load capacity of a masonry arch bridge can be significantly increased by bonding FRP plates to its intrados. This paper has presented tests conducted upon a large model two-span single-ring masonry arch bridge, topped by a sand fill. Each of the arches was initially loaded to determine their capacity prior to strengthening. Carbon FRP plates were then bonded to the intrados of the arches, and the arches were again tested to determine their strengthened response. Measurements were taken of both the global arch response (load and displacement) and of local behaviour (FRP strains and masonry crack widths) to achieve a detailed understanding of the FRP strengthened arch.

The FRP strengthening restrained the opening of the hinge cracks that form in a masonry arch and consequently reduce their deformation. By restraining the flexural crack opening required for a four-hinge mechanism, additional cracks are able to form within the masonry. The load capacity of the arch is increased because the FRP strengthening allows the line of thrust to move out of the extrados. Furthermore, masonry shear cracks (or mixed-mode flexure-shear cracks) are more likely to form when the four hinge-mechanism failure load is significantly increased by the FRP strengthening.

The capacity of the strengthened arches was governed by the behaviour of the bond between the masonry and the FRP plate. Debonding occurred at an intrados crack, and two debonding modes were observed. Flexural opening of the masonry crack resulted in shear debonding of the FRP on both sides of the crack, whereas shear deformation in the masonry results in peel debonding of the FRP to one side of the crack. Some load redistribution occurred between initial debonding and collapse for the arch strengthened using 3 FRP plates, but collapse occurred with little warning in the arch with 6 plates.

The FRP did not completely separate from the masonry arch at the ultimate load, but remained attached at either end. Thus, post-debonding tie action prevented catastrophic collapse and maintained the integrity of the arch despite it being greatly deformed. It should be noted, however, that whilst the capacity of the tie mechanism was above that of the unstrengthened arch, it was substantially below the strengthened capacity and hence collapse would have occurred immediately in a load-controlled situation.

ACKNOWLEDGEMENTS

The authors gratefully acknowledge the support of BASF for providing the CFRP strengthening materials; EPSRC (the UK Engineering and Physical Sciences Research Council) and Shell for their support of the first author with a Dorothy Hodgkin Postgraduate Award; and the Scottish Funding Council's support of the Joint Research Institute in Civil Engineering, part of the Edinburgh Research Partnership in Engineering and Mathematics (ERPem). This project would not have been possible without the technical support and expertise provided by Mr Jim Hutcheson and Mr Derek Jardine.

REFERENCES

[1] ACI. (2008). “ACI 440.2R-08. Guide for the Design and Construction of Externally Bonded FRP Systems for Strengthening Concrete Structures.” ACI Committee 440, Michigan, USA.

[2] Concrete Society (2004). “Design guidance for strengthening concrete structures using fibre composite materials.” Technical Report 55, The Concrete Society, Camberley, UK.

[3] Teng, J. G., Chen, J. F., Smith, S. T. and Lam, T. (2002). *FRP-strengthened RC structures*, Wiley & Sons, UK.

[4] De Lorenzis, L. (2008). “Strengthening of masonry structures with fibre-reinforced polymer (FRP) composites.” Strengthening and rehabilitation of civil infrastructures using fibre-reinforced polymer (FRP) composites, L. C. Hollaway and J. G. Teng, eds., CRC Press, USA.

[5] CNR. (2004). “CNR-DT 200/2004 Guide for the design and construction of externally bonded FRP systems for strengthening existing structures-materials, RC and PC structures, masonry structures.” Rome, Italy, Consiglio Nazionale delle Ricerche (English version).

[6] ACI. (2007). “ACI 440R-07. Report on Fiber-Reinforced Polymer (FRP) Reinforcement for Concrete Structures.” Michigan, USA.

[7] Heyman, J. (1966). "The stone skeleton." *International Journal of Solids and Structures*, 2, 249-279.

[8] Heyman, J. (1982). *The masonry arch*, Ellis Horwood limited Publ., Chichester.

[9] Foraboschi, P. (2004). “Strengthening of Masonry Arches with Fiber-Reinforced Polymer Strips.” *Journal of Composites for Construction*, 8(3), 191-202.

[10] Alcaino, P., and Santa-Maria, H. (2008). “Experimental Response of Externally Retrofitted Masonry Walls Subjected to Shear Loading.” *Journal of Composites for Construction*, 12(5), 489-498.

[11] ElGawady, M. A., Lestuzzi, P. and Badoux, M. (2005). “In-Plane Seismic Response of URM Walls Upgraded with FRP.” *Journal of Composites for Construction*, 9(6), 524-535.

[12] Stratford, T., Pascale, G., Manfroni, O. and Bonfiglioli, B. (2004). “Shear Strengthening Masonry Panels with Sheet Glass-Fiber Reinforced Polymer.” *Journal of Composites for Construction*, 8(5), 434-443.

[13] Triantafillou, T. C. (1998). “Strengthening of Masonry Structures Using Epoxy-Bonded FRP Laminates.” *Journal of Composites for Construction*, 2(2), 96-104.

[14] Turek, M., Ventura, C. E. and Kuan, S. (2007). “In-Plane Shake-Table Testing of GFRP-Strengthened Concrete Masonry Walls.” *Earthquake Spectra*, 23(1), 223-237.

[15] Albert, M. L., Elwi, A. E. and Cheng, J. J. R. (2001). “Strengthening of Unreinforced Masonry Walls Using FRPs.” *Journal of Composites for Construction*, 5(2), 76-84.

[16] Ehsani, M. R., Saadatmanesh, H. and Velazquez-Dimas, J. I. (1999). “Behavior of Retrofitted URM Walls under Simulated Earthquake Loading.” *Journal of Composites for Construction*, 3(3), 134-142.

[17] Hamoush, S. A., McGinley, M. W., Mlakar, P., Scott, D. and Murray, K. (2001). “Out-of-Plane Strengthening of Masonry Walls with Reinforced Composites.” *Journal of Composites for Construction*, 5(3), 139-145.

[18] Kuzik, M. D., Elwi, A. E. and Cheng, J. J. R. (2003). “Cyclic Flexure Tests of Masonry Walls Reinforced with Glass Fiber Reinforced Polymer Sheets.” *Journal of Composites for Construction*, 7(1), 20-30.

[19] Paquette, J., Bruneau, M. and Filiatrault, A. (2001). “Out-of-Plane Seismic Evaluation and Retrofit of Turn-of-the-Century North American Masonry Walls.” *Journal of Structural Engineering*, 127(5), 561-569.

[20] Drosopoulos, G. A., Stavroulakis, G. E. and Massalas, C. V. (2007). “FRP reinforcement of stone arch bridges: Unilateral contact models and limit analysis.” *Composites Part B: Engineering*, 38(2), 144-151.

[21] Bati, S. B., Rovero, L., and Tonietti, U. (2007). “Strengthening Masonry Arches with Composite Materials.” *Journal of Composites for Construction*, 11(1), 33-41.

[22] De Lorenzis, L., Dimitri, R. and La Tegola, A. (2007). “Reduction of the lateral thrust of masonry arches and vaults with FRP composites.” *Construction and Building Materials*, 21(7), 1415-1430.

[23] Bati, S.B. and Rovero L. (2008). “Towards a methodology for estimating strength and collapse mechanism in masonry arches strengthened with fibre reinforced polymer applied on external surfaces.” *Materials and Structures*, 41(7), 1291-1306.

[24] Valluzzi, M. R., Valdemarca, M. and Modena, C. (2001). “Behavior of Brick Masonry Vaults Strengthened by FRP Laminates.” *Journal of Composites for Construction*, 5(3), 163-169.

[25] Chen, J. F. (2002). “Load-bearing capacity of masonry arch bridges strengthened with fibre reinforced polymer composites.” *Advances in Structural Engineering*, 5, 37-44.

[26] Caporale, A., Luciano, R. and Rosati, L. (2006). “Limit analysis of masonry arches with externally bonded FRP reinforcements.” *Computer Methods in Applied Mechanics and Engineering*, 196(1-3), 247-260.

[27] BS EN 772-1:2000 (2000). “Methods of test for masonry units – Part 1: Determination of compressive strength.” British Standards Institution, London.

[28] BS ISO 1920-10:2009 (2009). “Testing of concrete - Part 10: Determination of static modulus of elasticity in compression.” British Standards Institution, London.

[29] BS 772-6 (2001). “Methods of test for masonry units – Part 6: Determination of bending tensile strength of aggregate concrete masonry units.” British Standards Institution, London.

[30] BS 1052-1:1999 (1999). “Methods of test for masonry - Part 1: Determination of compressive strength.” British Standards Institution, London.

[31] BS 1052-2:1999 (1999). “Methods of test for masonry - Part 2: Determination of flexural strength.” British Standards Institution, London.

[32] BS 1052-3:2002 (2002). “Methods of test for masonry - Part 3: Determination of initial shear strength.” British Standards Institution, London.

[33] Teng, J.G., Yuan, H. and Chen, J.F. (2006). “FRP-to-concrete interfaces between two adjacent cracks: theoretical model for debonding failure.” *International Journal of Solids and Structures*, 43(18-19), 5750-5778.

[34] Chen, J.F., Yuan, H. and Teng, J.G. (2007). "Debonding failure along a softening FRP-to-concrete interface between two adjacent cracks in concrete members.” *Engineering Structures*, 29(2), 259-270.

[35] White D.J., Take W.A. & Bolton M.D. 2003. “Soil deformation measurement using particle image velocimetry (PIV) and photogrammetry”, *Geotechnique*, 53 (7), 619-631

[36] Chen J.F. & Teng J.G. (2001). “Anchorage models for FRP and steel plates bonded concrete”, *Journal of Structural Engineering*, 127(7), 784-791

[37] De Lorenzis, L., Zavarise, G. (2009). “Interfacial stress analysis and prediction of debonding for a thin plate bonded to a curved substrate.” *International Journal of Non-Linear Mechanics*, 44(4), 358-370.

[38] De Lorenzis, L., Zavarise, G. (2010). “Debonding analysis of thin plates from curved substrates.” *Engineering Fracture Mechanics*, 77(16), 3310-3328.

Table 1 Properties of the masonry materials

	Material property (number of samples)		Value	Direction relative to bed joints	Test standard
Brick properties	Compressive strength (7)	f_{cb} (MPa)	58.2	Perpendicular	BS EN 772-1 [27]
	Modulus of elasticity (7)	E_b (MPa)	16600	Perpendicular	Based on BS ISO 1920-10 [28]
	Flexural tensile strength (6)	f_{tb} (MPa)	8.84	Parallel	BS 772-6 [29], in 3 point bending
Masonry properties	Compressive strength (3)	f_{cm} (MPa)	25.0	Parallel	BS 1052-1 [30]
	Modulus of elasticity (3)	E_m (MPa)	11800	Parallel	Based on BS ISO 1920-10 [28]
	Flexural tensile strength (3)	f_{tm} (MPa)	0.1	Perpendicular	BS 1052-2 [31], in 4 point bending
Mortar joint in shear	Initial shear strength (17)	f_{v0} (MPa)	0.39	Across bed joint	BS 1052-3 [32], Type 1
	Internal angle of friction (17)	α (°)	43		

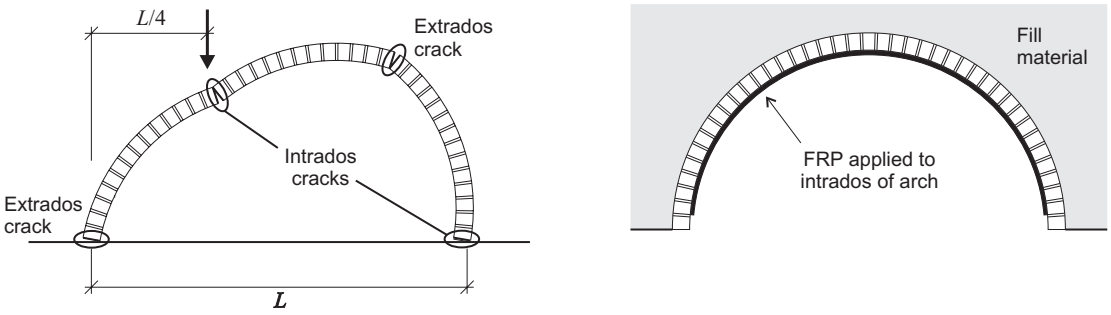

Figure 1 - The use of FRP strengthening to resist the formation of the four-hinge mechanism in a masonry arch

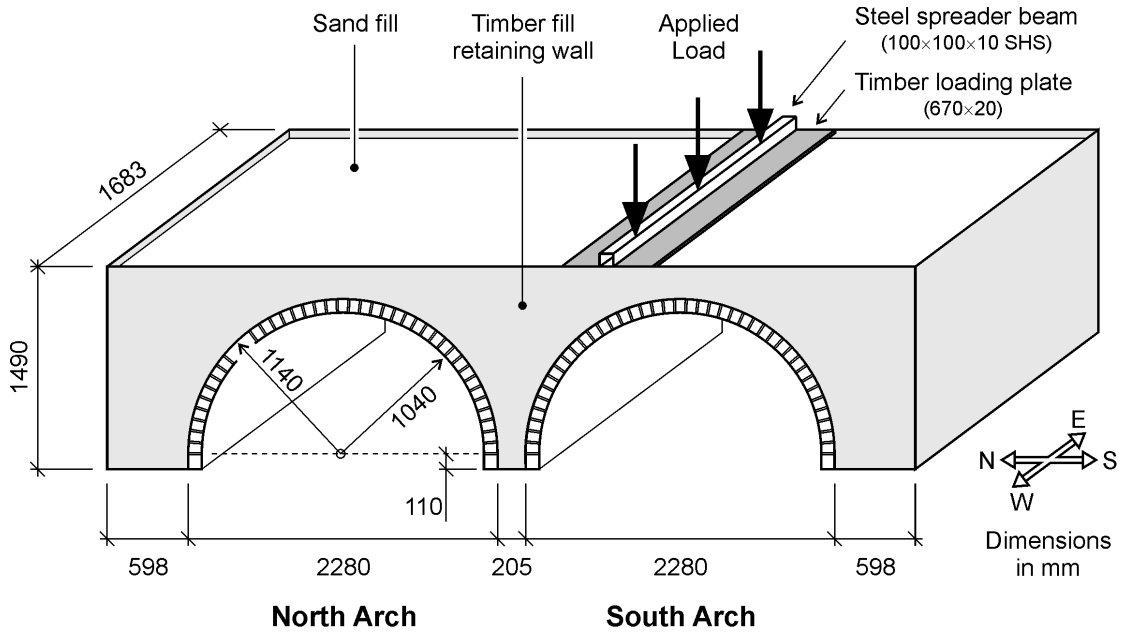

(a) Schematic arrangement

(b) Photograph, taken from the west side after strengthening

Figure 2 - General arrangement of the two-span arch bridge

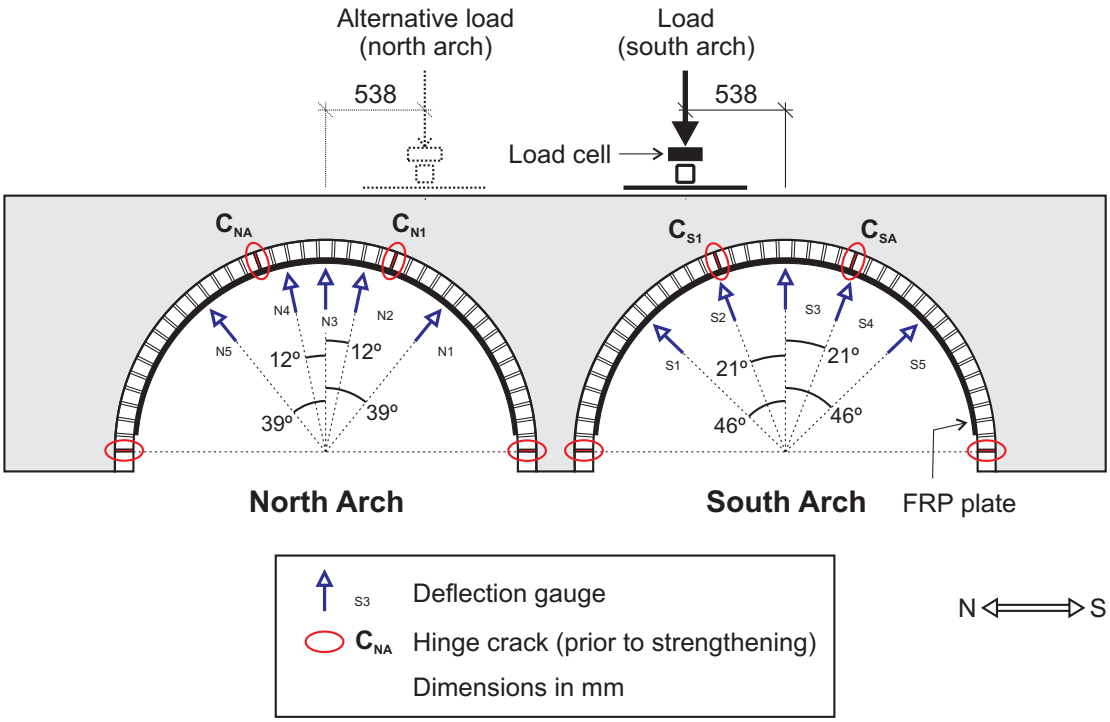

Figure 3 - The western elevation of the arches, showing the strengthening plates, instrumentation, and crack locations prior to strengthening

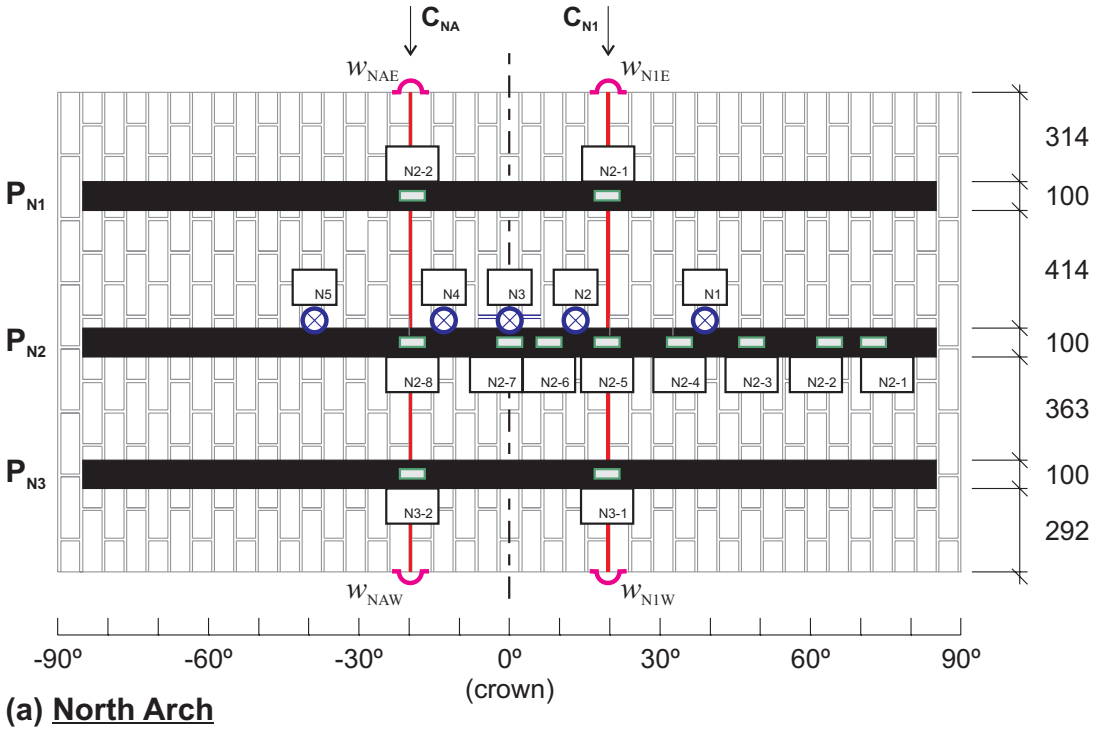

(a) North Arch

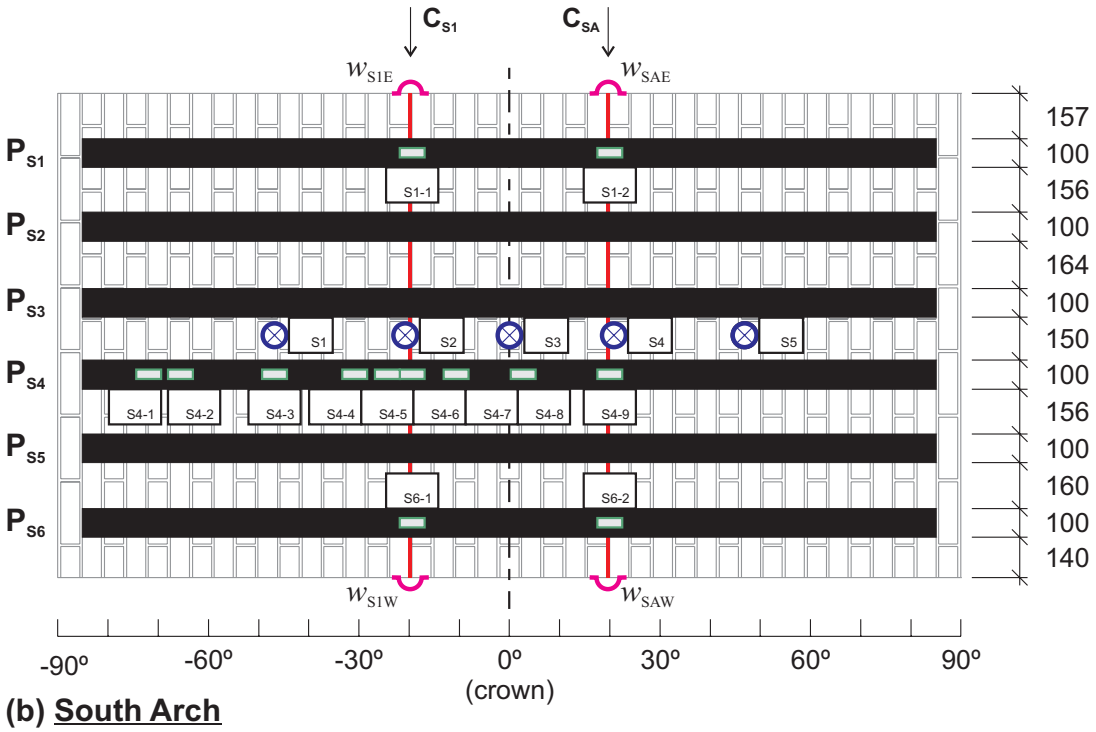

(b) South Arch

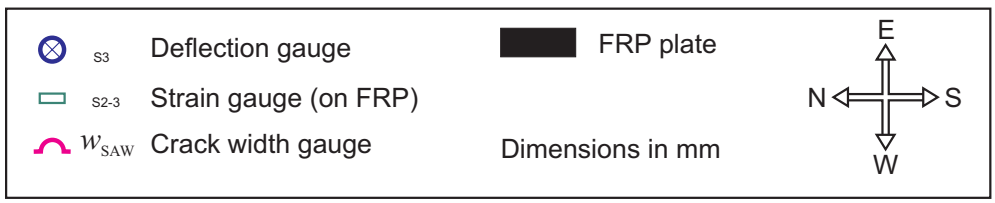

Figure 4 - Developed plan view of the two arches' intrados, showing the strengthening plates, instrumentation crack locations prior to strengthening

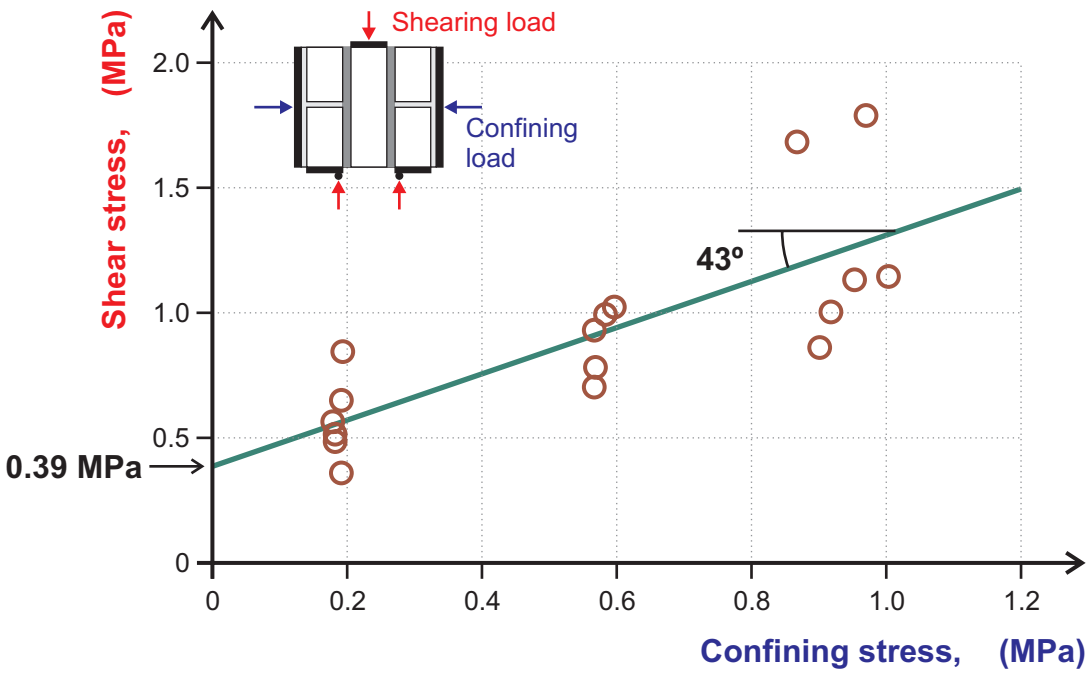

Figure 5 - Shear strength and internal friction angle of the masonry bed joints: individual test results and linear regression

(a) Intrados Crack C_{N1} (b) Extrados Crack C_{NA}

Figure 6 - Typical hinge cracks, viewed from the west

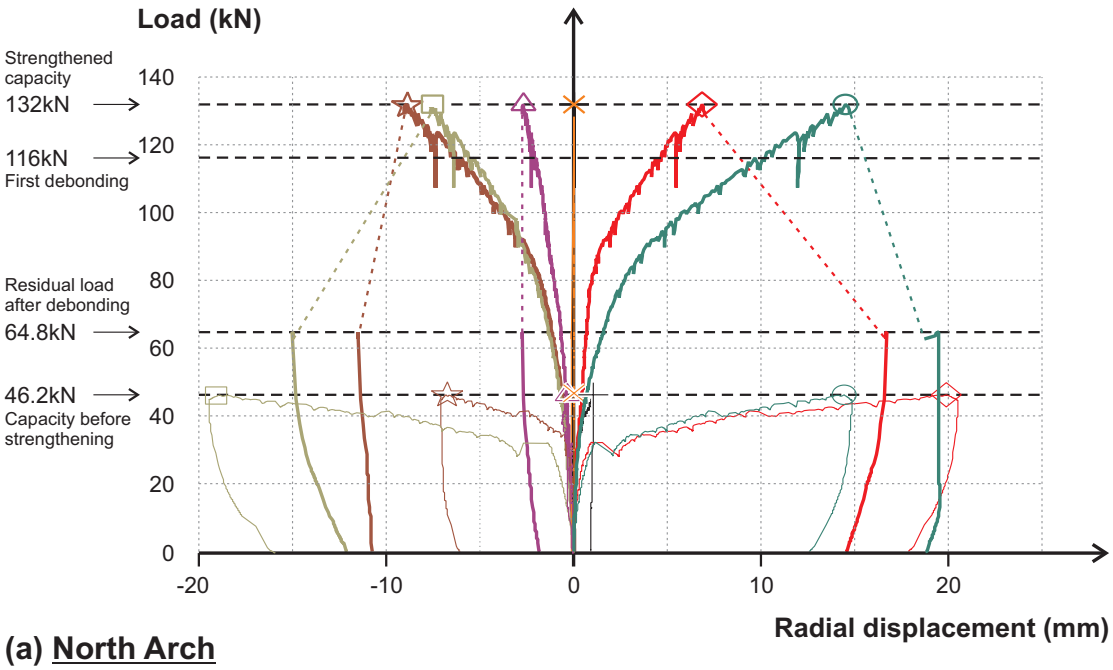

(a) North Arch

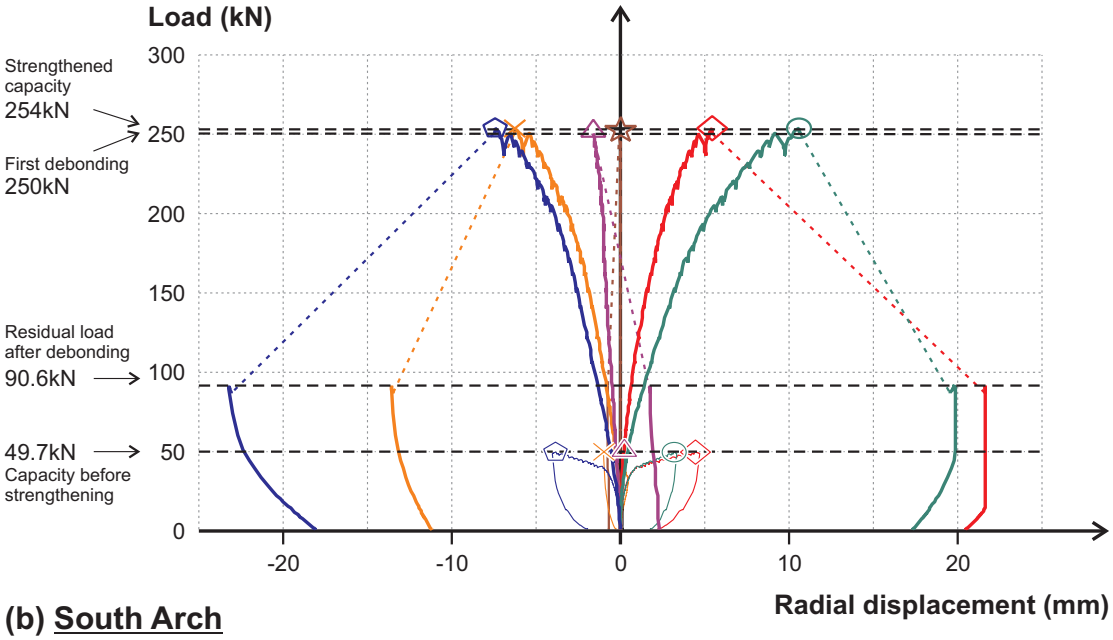

(b) South Arch

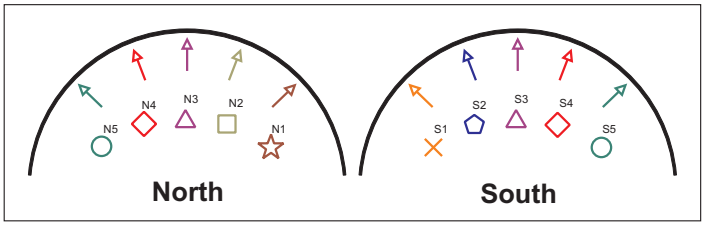

Figure 7 - Load vs. radial displacement curves for both strengthened and unstrengthened arches

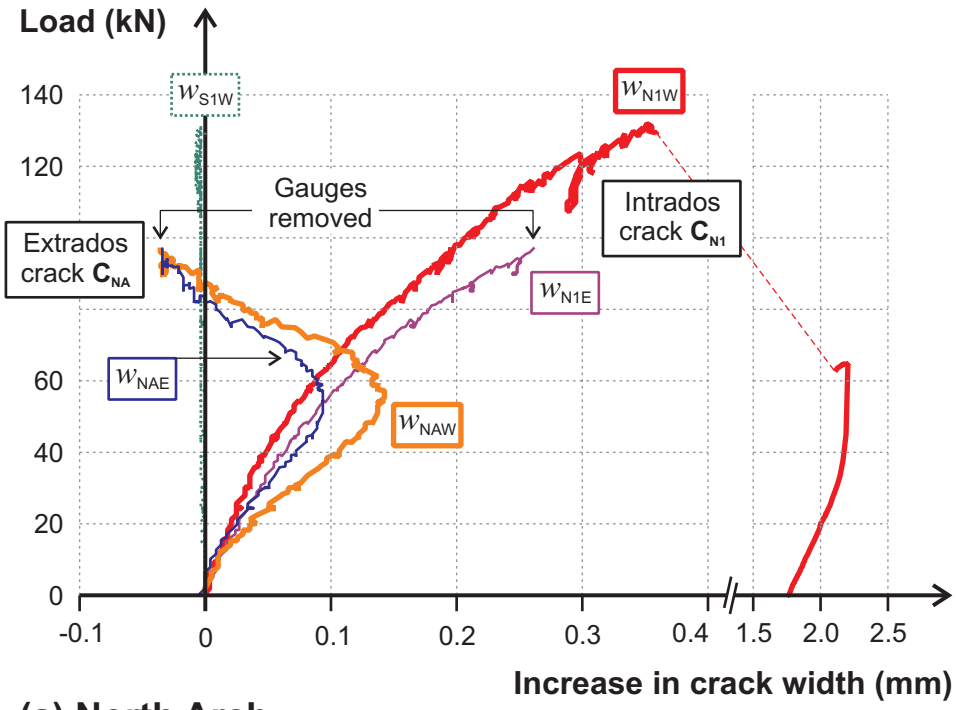

(a) North Arch

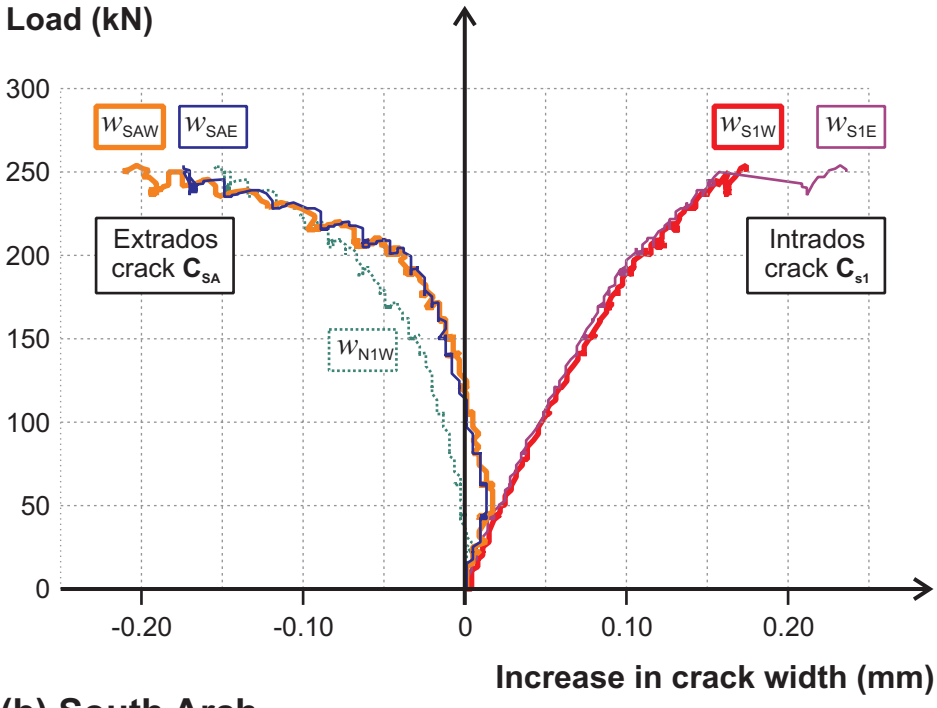

(b) South Arch

Figure 8 - Load vs. crack width increase for the arches after strengthening

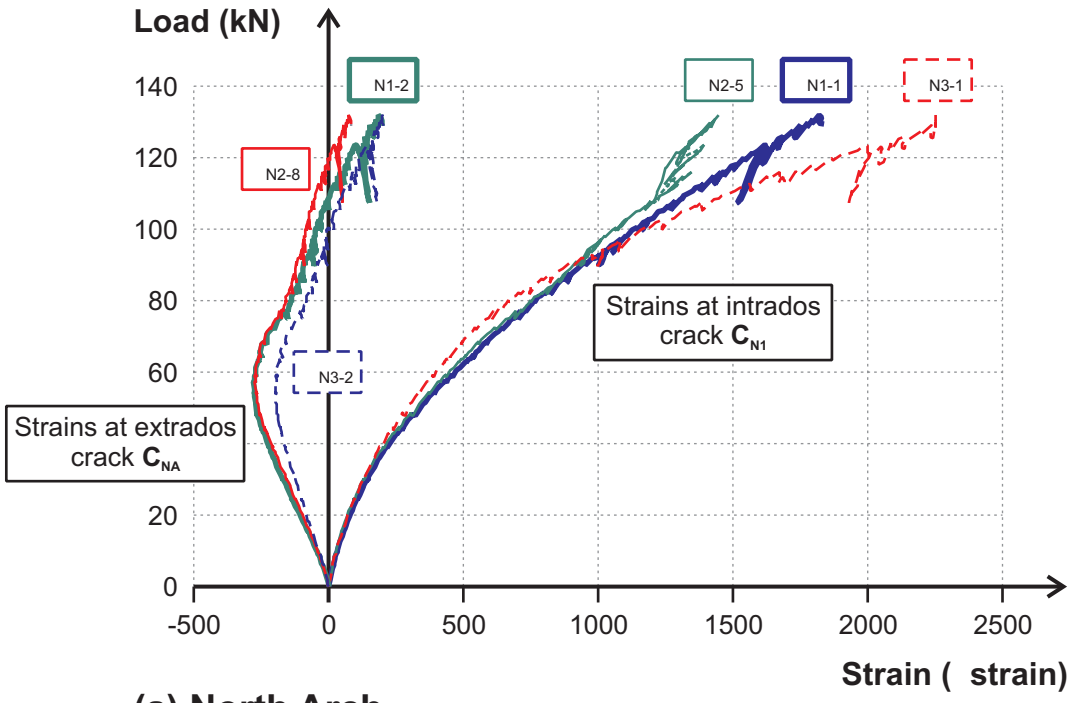

(a) North Arch

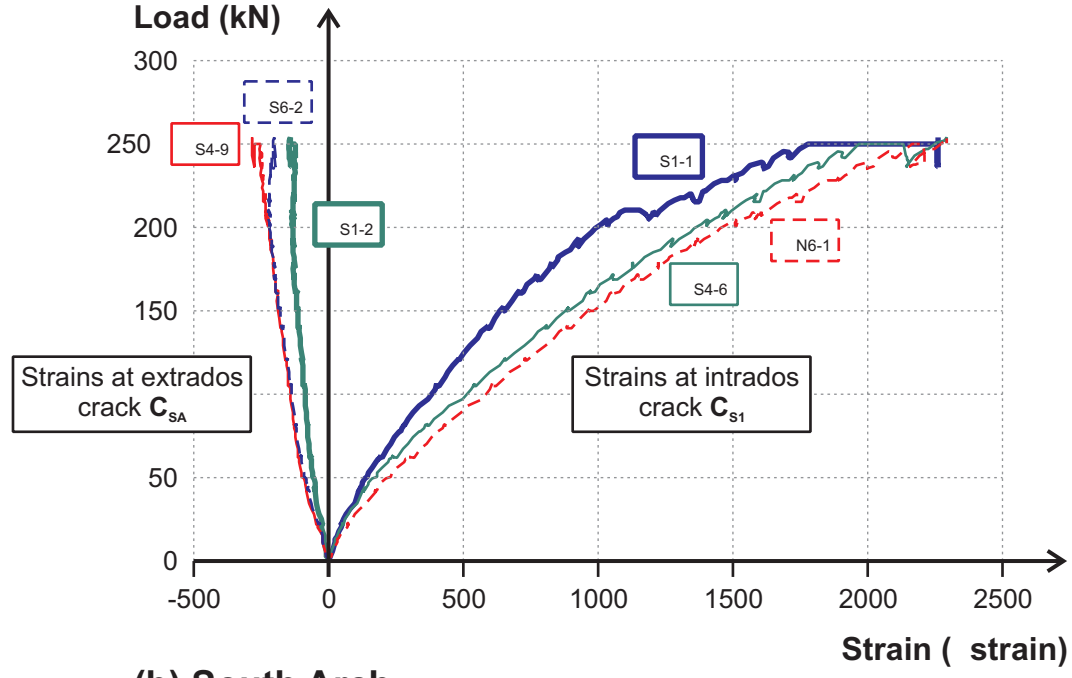

(b) South Arch

Figure 9 - Development of FRP longitudinal strain at the cracks

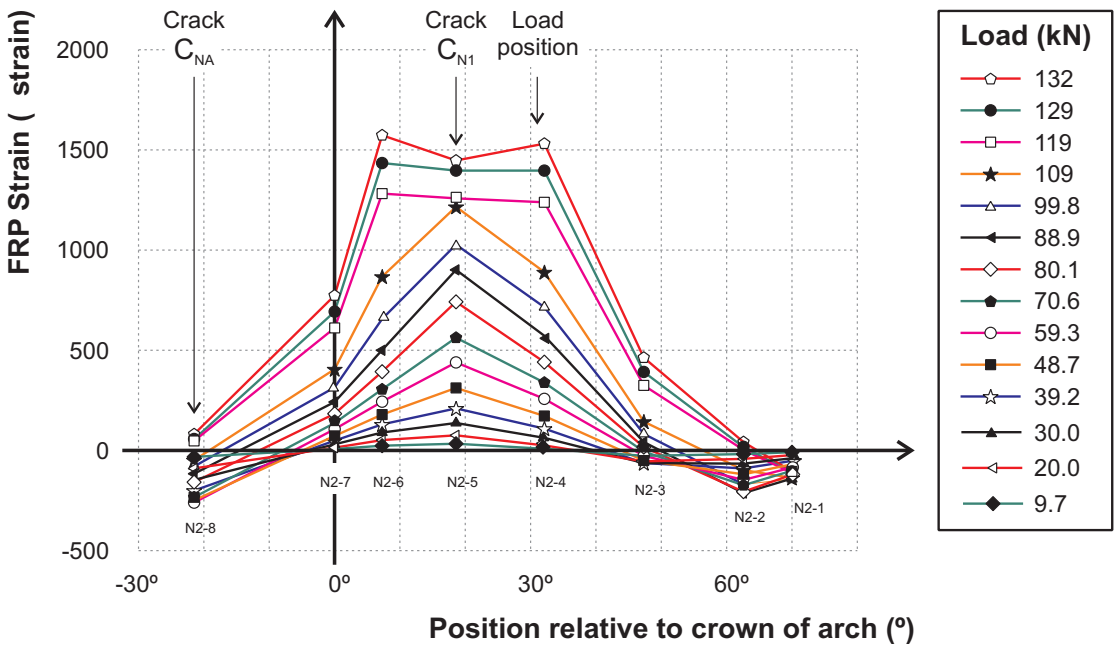

(a) North Arch: Plate P_{N2}

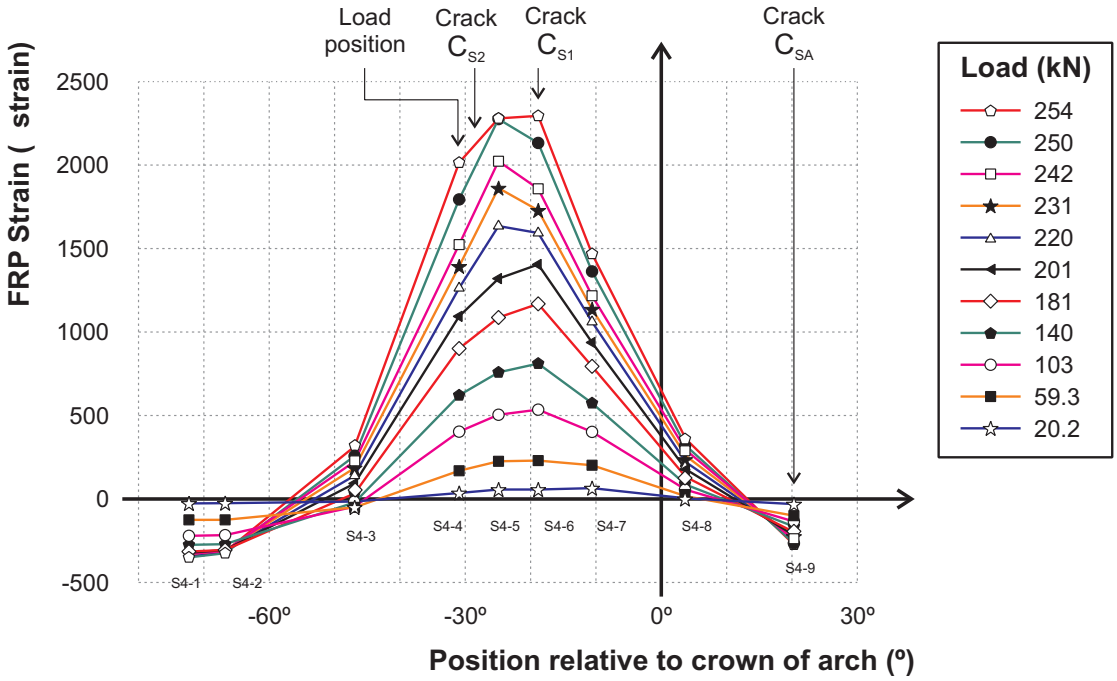

(b) South Arch: Plate P_{S4}

Figure 10 - Distributions of longitudinal FRP strain along the central plates at different applied loads

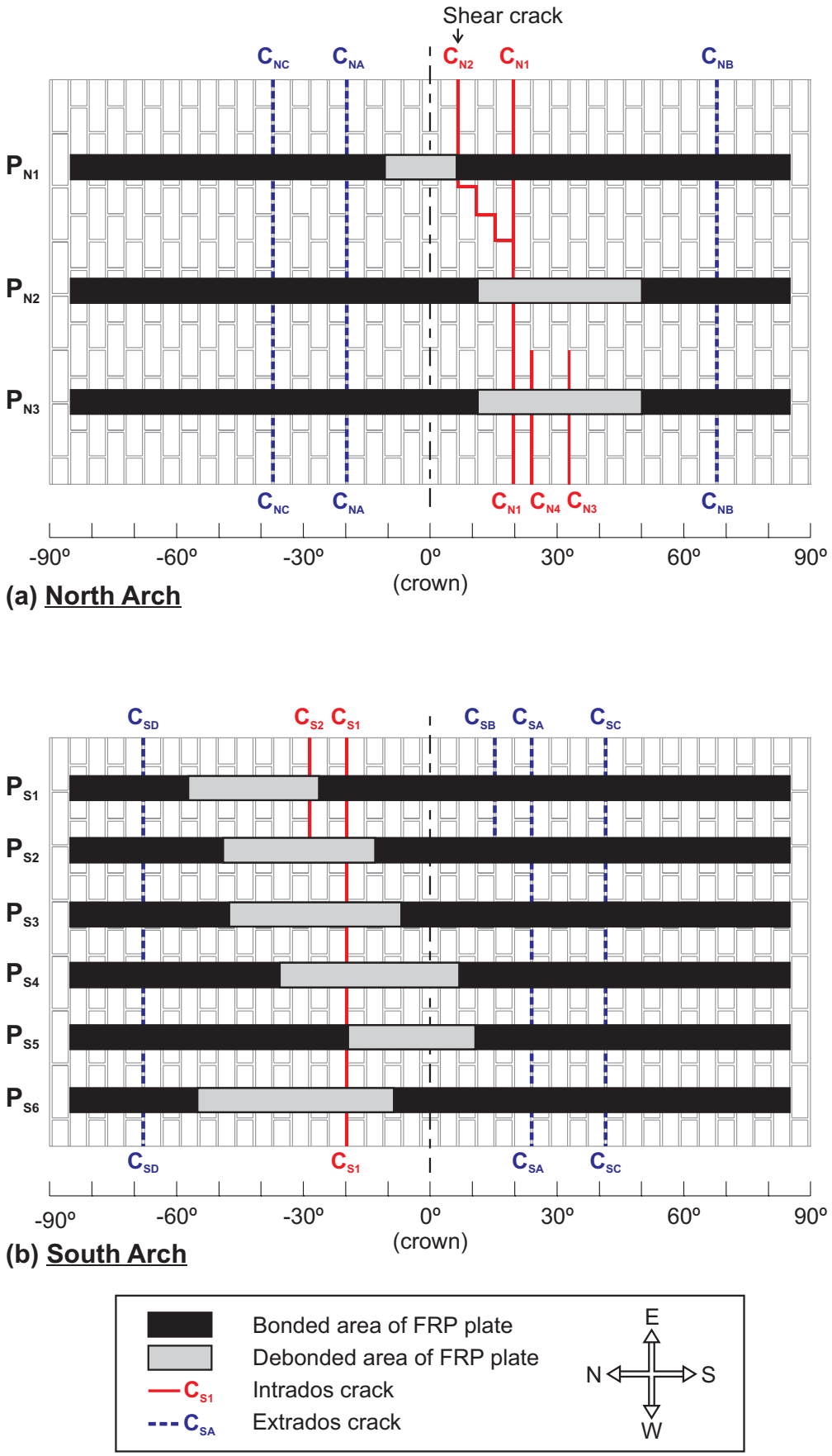

Figure 11 - Developed plan view of the arches showing crack locations in the masonry and the extent of debonding after failure of the strengthening system

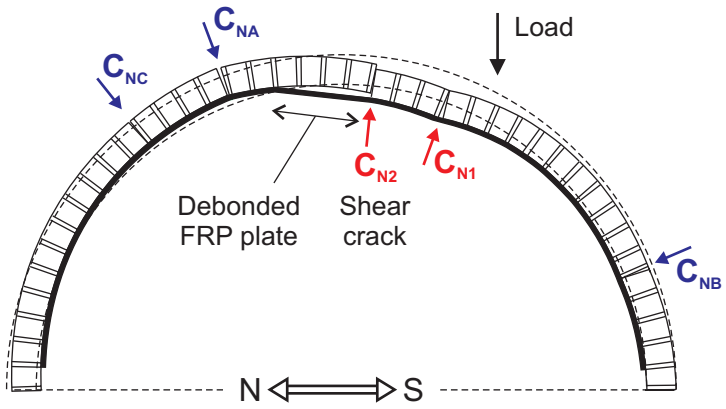

(a) Plate P_{N1}

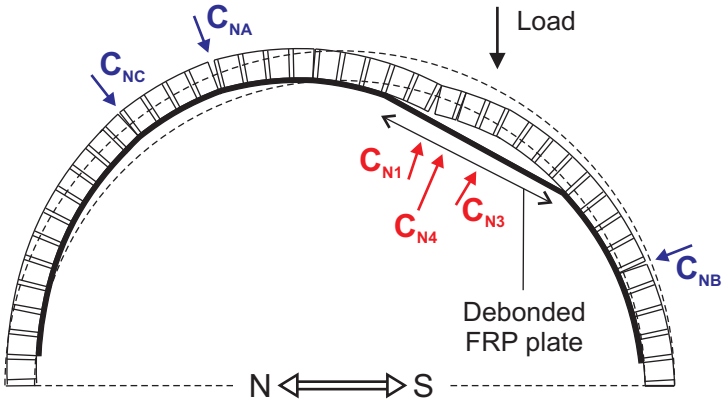

(b) Plates P_{N2} and P_{N3}

Figure 12 - Sections along the FRP plates in the north arch, showing the failure mechanism post peak load

(a) Shear crack and debonding at Plate P_{N1}

(b) Flexural crack and debonding at Plate P_{S4}

Figure 13 - Detailed view of debonding of the FRP from the masonry

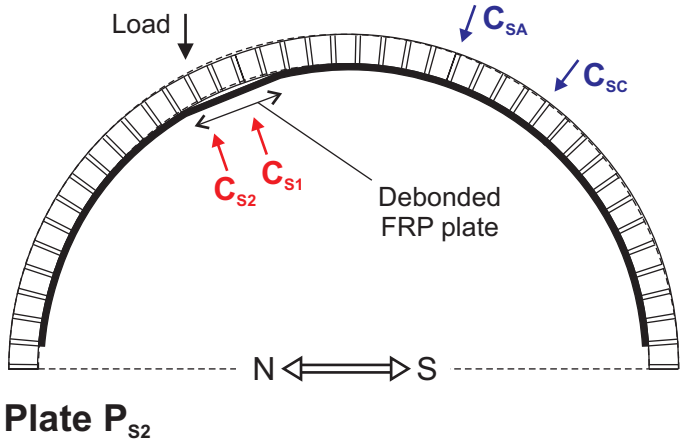

Figure 14 - Plate P_{S2} on the south arch after initial debonding (250kN)

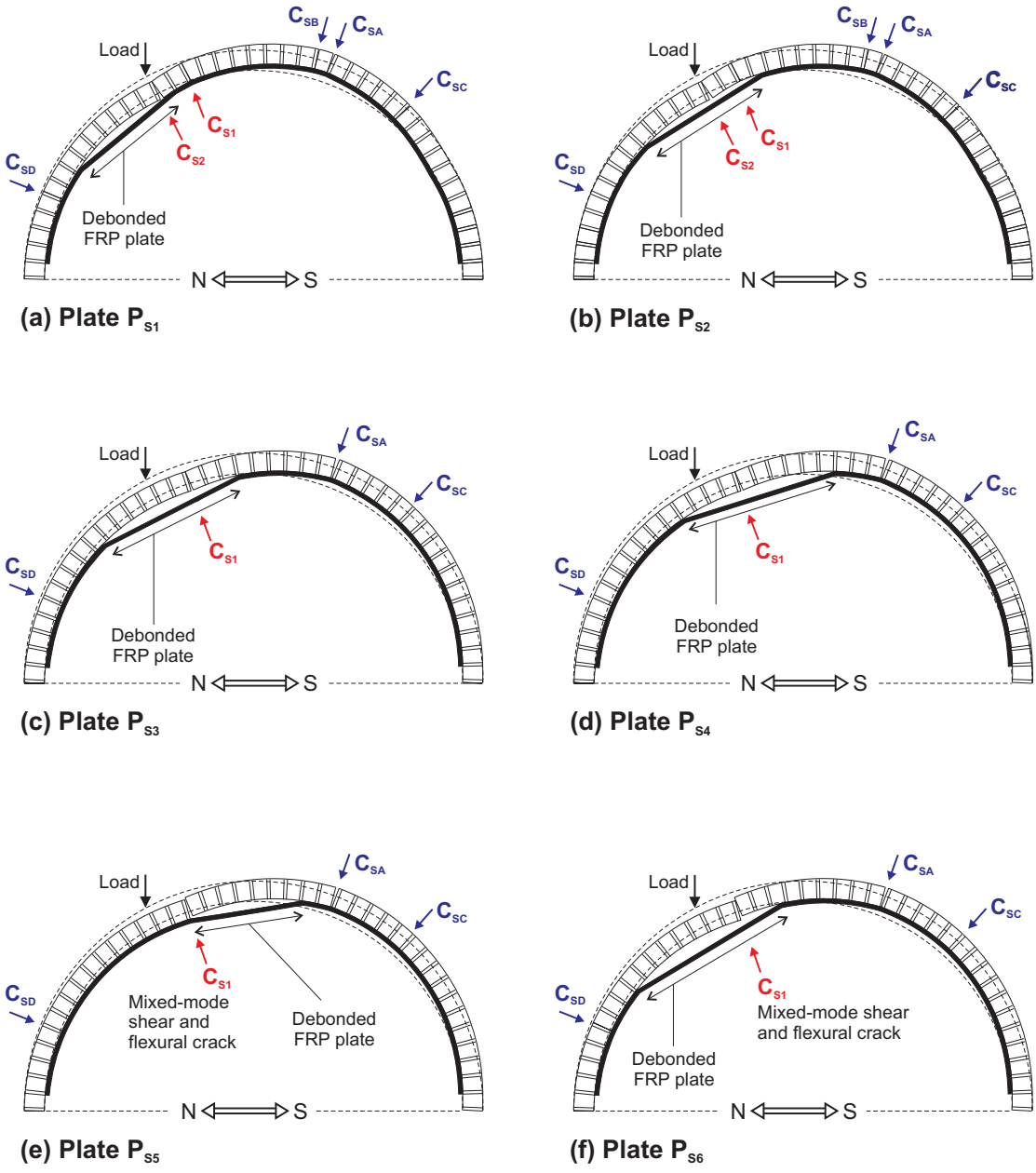

Figure 15 - The deformed shape of the south arch and position of FRP post peak load

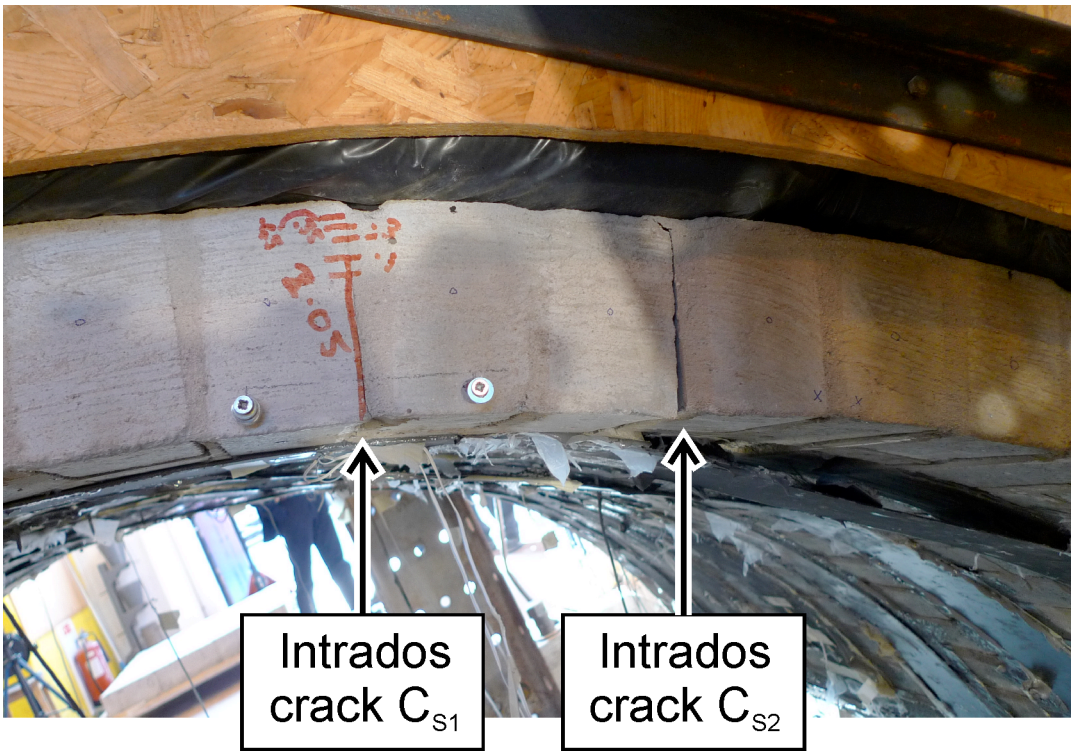

Figure 16 - Intrados cracks C_{S1} and C_{S2} on the east side of the south arch, following the formation of crack C and closing up of C_{S1}

Figure 17 - Mixed-mode flexural and shear failure at intrados crack (C_{S1}), on the west side of the bridge

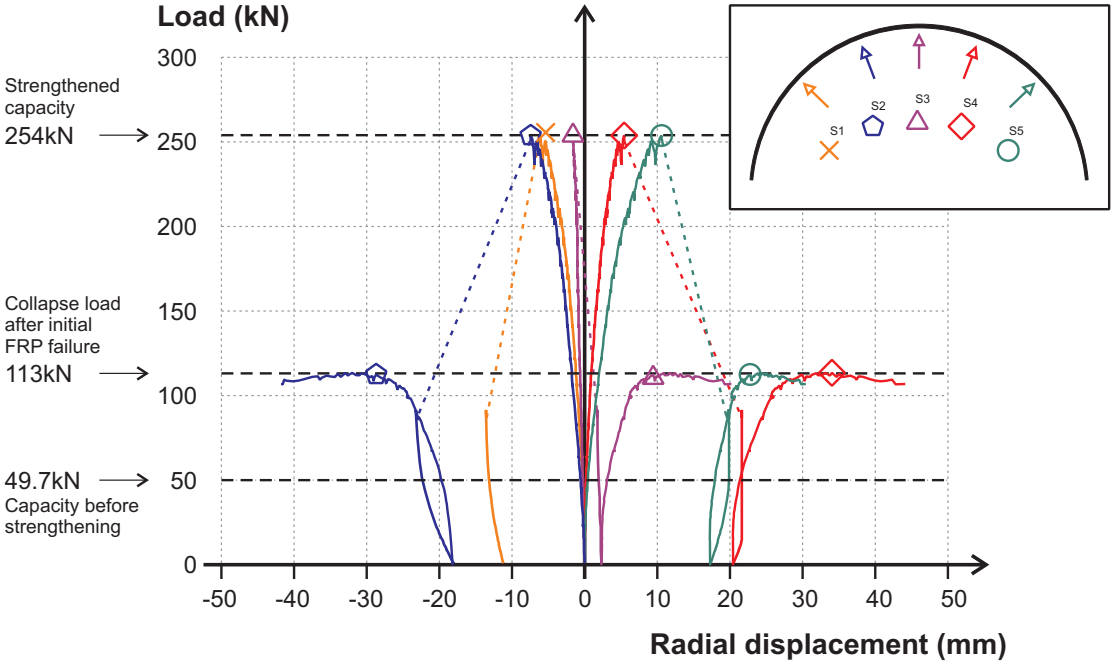

Figure 18 - Load vs. radial displacement curves for the south arch, including the collapse test after debonding failure of the FRP strengthening